



Fabrication of Co–Ni–P film with excellent wear and corrosion resistance by electroplating with supercritical CO₂ emulsion

Can-sen LIU^{1,2}, Feng-hua SU¹, Ji-zhao LIANG¹

1. School of Mechanical and Automotive Engineering,

South China University of Technology, Guangzhou 510640, China;

2. School of Materials and Energy, Guangdong University of Technology, Guangzhou 510006, China

Received 18 January 2018; accepted 3 June 2018

Abstract: To avoid the defects caused by the hydrogen evolution and improve the corrosion and wear properties of the electroplated films in the traditional aqueous bath electrodeposition, a supercritical carbon dioxide (Sc-CO₂) emulsion was proposed to electrodeposite ternary nanocrystalline Co–Ni–P alloy films. Microstructure, corrosive and tribological properties of the Co–Ni–P films were investigated and compared with the ones electroplated by conventional method. The results show that the Co–Ni–P films produced with Sc-CO₂ assisted electrodeposition exhibit a more compact microstructure. The preferred orientation plane of hcp (110) for the Co–Ni–P films produced in conventional aqueous bath is changed to be hcp (100) for the one prepared in emulsified Sc-CO₂ bath. The microhardness, corrosion resistance and tribological properties of the Co–Ni–P films are substantially improved with the assistance of Sc-CO₂ in the electrodeposition bath.

Key words: Co–Ni–P film; electrodeposition; supercritical carbon dioxide; wear; corrosion

1 Introduction

Material failures such as fatigue fracture, wear and corrosion always occur on surfaces, causing enormous energy and economic loss [1]. Surface film as protective layer is an effective approach to increase the lifetime of mechanical components. Hard chromium (Cr) film has been used extensively as protective layer for over a century owing to its attractive properties, including high hardness, corrosion protection and wear resistance. However, Cr film presents harmful effects on the environment and the public health because of its carcinogenic and toxic plating solution [2].

Ni–P and its composite films have been considered as alternatives to hard Cr films for anti-wear and anti-corrosion applications [3–7]. However, friction coefficient in the range of 0.45–0.7 is observed for the Ni–P films sliding against different counterface materials under dry conditions. MA et al [8] reported that electrodeposited Co-rich Ni–Co alloy films exhibited

low friction coefficient and improved anti-wear property. It is expected that the incorporation of Co into the Ni–P film can improve the friction-reducing and anti-wear ability of the resulting films. The Co–Ni–P films were always produced by electroless plating [9] and electrodeposition [10]. Compared with electroless plating, electrodeposition is a cost-effective technique to prepare films with desirable structure and properties [11–13]. The Co–Ni–P films are normally used as magnetic recording media [14], microwave absorptive materials [15] and electrocatalytic materials for water electrolysis [16]. However, the tribological and corrosive properties of the Co–Ni–P films receive little attention despite the significance for their industrial application. Besides, evolution of hydrogen (H₂) is an inevitable size reaction during the electrodeposition process in aqueous electrolyte. H₂ gas bubbles adsorbed on the cathode induce defects, which affects the properties of the deposits and restricts its applications under wear and corrosion condition.

Evolution problem of H₂ can be overcome by

Foundation item: Project (2015A030306026) supported by the Natural Science Funds for Distinguished Young Scholar of Guangdong Province, China; Project (51275176) supported by the National Natural Science Foundation of China; Project (2016A010102009) supported by the Science and Technology Planning of Guangdong Province, China; Project (201707010055) supported by the Science and Technology Planning of Guangzhou City, China

Corresponding author: Feng-hua SU; Tel: +86-20-82313996; E-mail: fhsu@scut.edu.cn
DOI: 10.1016/S1003-6326(18)64895-2

introducing supercritical CO₂ (Sc-CO₂) in the electro-deposition process. Desorption of H₂ bubbles from the cathode surface is enhanced by application of Sc-CO₂ [17], because the solubility of H₂ in Sc-CO₂ is higher than that in the aqueous solution [18]. CO₂ is also nontoxic, inexpensive and the critical point of Sc-CO₂ is relatively low, which endows Sc-CO₂ in electroplating application attractive and advantageous. Many researches have demonstrated that electroplating in Sc-CO₂ emulsion is effective in reducing defects formation, grain refinement and hardness enhancement for the prepared films. CHANG et al [19] reported that the bright Ni film electroplated with Sc-CO₂ emulsion using additive-free Watts bath displayed lower surface roughness and smaller grain size than the one electroplated through conventional method. CHIU et al [20] confirmed that the microhardness, wear and corrosion resistance of the pure Ni and Ni–Al₂O₃ films fabricated in the emulsified Sc-CO₂ bath were substantially increased. LUO et al [21] demonstrated that Sc-CO₂ was effective in eliminating defects formation in the Co films. Our previous work [22] also noted that Sc-CO₂ assisted electrodeposition greatly improved the microstructure and properties of the Co–Ni film when being compared with the conventional electrodeposition technique.

In this work, ternary nanocrystalline Co–Ni–P alloy films were firstly electrodeposited from an emulsified Sc-CO₂ bath. The morphology, crystal structure, microhardness, corrosion and wear resistances for the Co–Ni–P films were systemically evaluated and compared with those of the films electrodeposited in conventional aqueous bath.

2 Experimental

2.1 Electrodeposition of Co–Ni–P films

A high-pressure cell made of stainless steel was manufactured for the electrodeposition in emulsified Sc-CO₂ bath. The autoclave system and the apparatus used for the Co–Ni–P films electrodeposition have been described elsewhere [22]. A Co plate (purity of 99.9%) and a brass plate with size of 20 mm × 40 mm were used

as the anode and working cathode, respectively. Distance between the cathode and anode was kept at 20 mm. Prior to plating, the surface of the brass plate was mechanically polished using abrasive water paper from 600 to 1500 grade and sequentially cleaned ultrasonically in distilled water and acetone to remove contaminations on the substrate surface. The bath compositions and the operational parameters for electrodepositing Co–Ni–P film are given in Tables 1 and 2. The surfactant used was polyoxyethylene lauryl ether (CAS No. 9002-92-0). Two types of electrodeposition baths, conventional and emulsified Sc-CO₂, were used in this investigation. For conventional electroplating, specimens were prepared at ambient pressure and 50 °C in the conventional aqueous electrolyte without the addition of surfactant. The emulsified Sc-CO₂ bath was prepared by purging pressurized CO₂ at 10 MPa into the conventional aqueous electrolyte with addition of surfactant to ensure to obtain an emulsified fluid. The bath consisted of 100 mL conventional aqueous electrolyte and 50 mL Sc-CO₂ fluid. The electrodeposition was conducted using an intelligent multiwave electroplating equipment supplied by Handan Dashun Electroplating Equipment Co., Ltd., China. The Co–Ni–P films electroplated in conventional aqueous bath and in emulsified Sc-CO₂ bath are abbreviated as Co–Ni–P-I and Co–Ni–P-II, respectively.

2.2 Characterization of Co–Ni–P films

The morphologies of the Co–Ni–P films surface were observed using a Quanta 200 scanning electron microscopy (SEM). The element compositions of the Co–Ni–P films were analyzed by energy dispersive X-ray spectroscopy (EDS) microanalyzer attached with the Quanta 200 SEM. The crystal structures of the as-deposited films were characterized by a Philips X'pert X-ray diffractometer (XRD, Cu K_α radiation) operating at 40 kV and 40 mA over the 2θ range of 10°–90°. The microhardness was measured on a Vicker's microhardness tester with a load of 25 g applied for 10 s. The average value from eight replicates for each kind of specimen was reported.

Table 1 Bath compositions for electrodeposition of Co–Ni–P films (g/L)

Cobalt sulfate	Nickel sulfate	Sodium hypophosphite	Boric acid	Sodium citrate	Lauryl sodium sulfate	Saccharin sodium
30	30	10	40	30	0.1	1.0

Table 2 Operational parameters for electrodeposition of Co–Ni–P films

φ(Surfactant)/%	pH	Temperature/°C	Current density/(A·dm ⁻²)	Agitating speed/(r·min ⁻¹)	Deposition time/min	Pressure/MPa	Volume of dense carbon dioxide (minimum purity of 99.9%)/mL
1.0	4.8	50	2.5	400	30	10	50

The friction and wear behaviors of the Co–Ni–P films were evaluated on a ball-on-disk tribometer. The test was carried out under the following conditions: a sliding speed of 0.188 m/s, an applied load of 4.0 N for 20 min, the counterpart GCr15 steel ball with diameter of 4.0 mm, room temperature and ambient humidity. After the wear tests, the wear tracks were measured using a Talysurf CLI 1000 surface profile measurement system to achieve the wear volume. The wear rates of all the films were calculated from $K=V/(S \cdot F)$, where V is the wear volume (mm^3), S the total sliding distance (m) and F the normal load (N). Three replicate friction and wear tests were carried out for each specimen and the average was reported with their errors. After sliding, the worn surfaces of the films and their corresponding counterpart balls were analyzed using the Quanta 200 SEM.

Electrochemical corrosion test was carried out in a three-electrode cell. Platinum plate and saturated calomel electrode (SCE) electrode were used as the counter and reference electrode, respectively. The as-fabricated Co–Ni–P films were used as the working electrode. Measurements were performed by an electrochemical workstation (CorrTest CS310, Wuhan Corr Test Instrument Co. Ltd., China) at room temperature with 3.5% (mass fraction) NaCl solution as corrosive medium. Before electrochemical tests, samples were mounted

using paraffin wax with surface area of 1 cm^2 exposed to the corrosive medium. All the samples were immersed for 30 min, allowing the system to be stabilized before the potentiodynamic polarization and electrochemical impedance spectroscopy (EIS) tests. The potentiodynamic polarization curves were recorded at a sweep rate of 0.5 mV/s from -200 to 200 mV versus the open circuit potential. As to EIS measurements, the employed amplitude of the sinusoidal signal was 10 mV, and the frequency range studied was from 1×10^5 to 1×10^{-2} Hz. The average value from three replicates for each kind of specimen was reported.

3 Results and discussion

3.1 Microstructure and composition of Co–Ni–P films

Surface and cross-sectional SEM images of the Co–Ni–P films electroplated by two different techniques are depicted in Fig. 1. The Co–Ni–P film deposited by the conventional electrodeposition (Co–Ni–P-I) displays an uneven surface with more particles and smaller groove than the one electroplated in emulsified Sc- CO_2 bath (Co–Ni–P-II), as shown in Figs. 1(a) and (b). Additionally, numbers of pinholes/defects and an obvious interface between the film and substrate are observed on the cross-sectional view of the Co–Ni–P-I

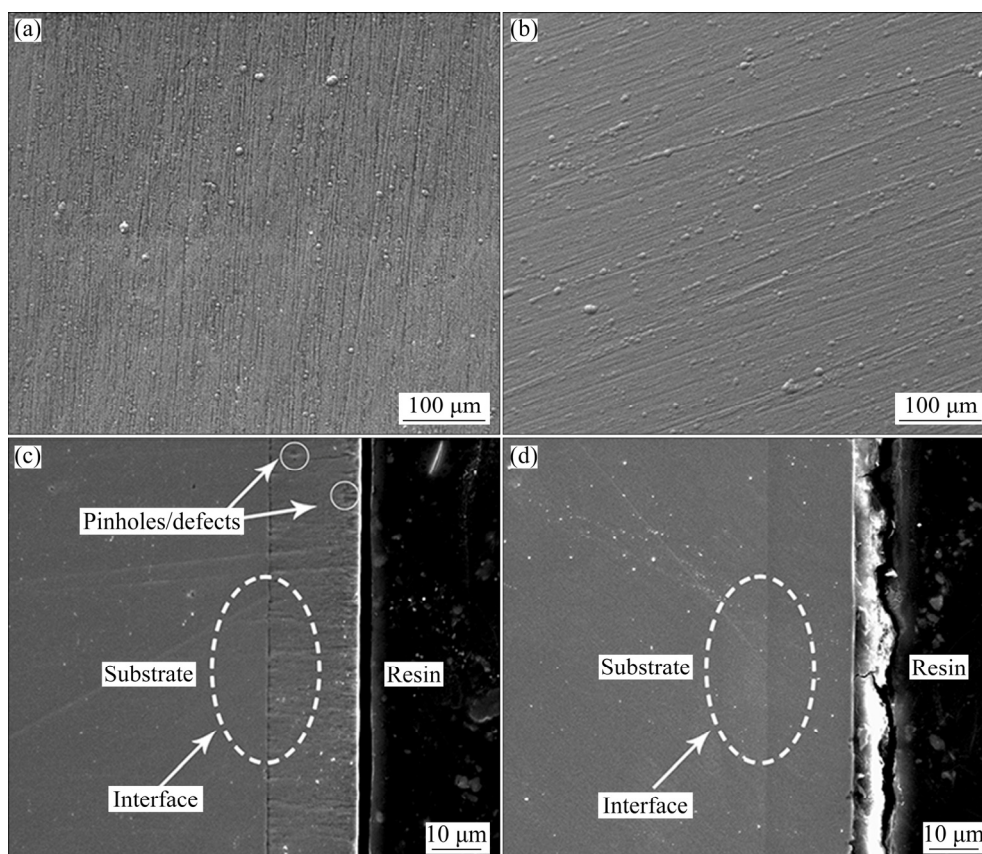


Fig. 1 SEM images of surface (a, b) and cross-section (c, d) for Co–Ni–P films electroplated by different techniques: (a, c) Co–Ni–P-I; (b, d) Co–Ni–P-II

film (Fig. 1(c)). In contrast, the Co–Ni–P-II film exhibits a compact structure and strong bonding between the film and substrate is achieved (Fig. 1(d)). No sharp interfaces can be seen from the cross-sectional view of the Co–Ni–P-II film. In common electroplating in aqueous electrolyte, the cathode reactions include metal ion and H^+ reduction simultaneously. H_2 bubbles formed near the cathode will absorb onto the surface of the cathode and induce void defects in the plated films. CO_2 is non-polar, solubility of H_2 is high in CO_2 and desorption of H_2 gas bubbles from the surface of cathode could be significantly enhanced in Sc- CO_2 . In a consequence, Sc- CO_2 emulsion electrodeposition technique produces deposits free of pinholes/defects and the as-deposited Co–Ni–P film displays a more compact structure and stronger bonding with the substrate than the conventional one. Previous studies [19,23] have performed an electroplating without Sc- CO_2 at the same pressure and temperature and using an electroplating solution only under surfactants doping to confirm that the quality of the film has not originated from high pressure nor the surfactants. Meanwhile, it can be seen that the thickness of the Co–Ni–P films is approximate 17 μm and the Co–Ni–P-II film is slightly thinner than Co–Ni–P-I film, which suggests that the film growth rate is lower in the electroplating carried out in emulsified Sc- CO_2 bath than in the conventional aqueous bath. This finding is consistent with reports previously [20,24]. The micelle formed in the emulsified Sc- CO_2 bath causes a reduction in the number of active sites at the substrate/electrolyte interface for electrochemical reaction [19]. Moreover, carbonic acid is formed when CO_2 is dissolved in water, which increases the concentration of H^+ in electrolyte. During electrodeposition, the rapid reduction of increased amounts of H^+ ions to H_2 causes a lower current efficiency. As a result, the deposition rate is hindered and the corresponding film is thinner.

Composition of the Co–Ni–P films electroplated by the two different techniques is shown in Fig. 2. It is clearly observed that the Co content in the Co–Ni–P films is always higher than that in the electrolyte, in spite of the electrodeposition technique. According to Brenner's definition [25], this phenomenon is widely recognized as an anomalous electroplating type since the less noble metal (Co: -0.277 V versus standard hydrogen electrode) is deposited preferentially than the more noble metal (Ni: -0.257 V versus standard hydrogen electrode) and its percentage in the deposit is obviously higher than that in the electrolyte (Table 1). Generally, the anomalous deposition is owing to hydrogen evolution, because of the side reaction of metal reduction at the cathode surface. The hydrogen evolution consumes protons, and consequently increases the local concentration of hydroxyl ions. The increase in the concentration of

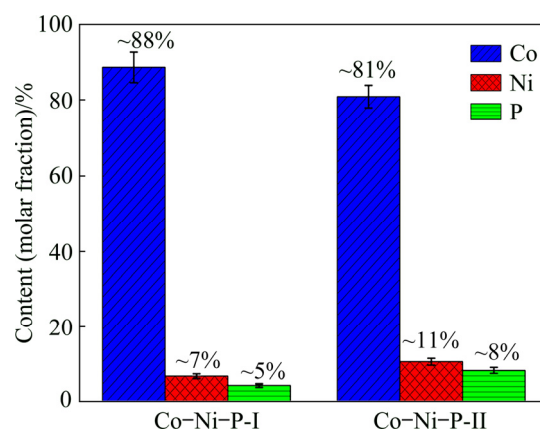


Fig. 2 Composition of Co–Ni–P films deposited by different techniques

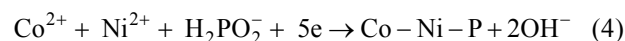
hydroxyl ion results in the formation and adsorption of metal hydroxide ions on cathode surface, favoring the anomalous deposition. Resulting from the higher adsorption ability of $Co(OH)^+$ than $Ni(OH)^+$ on the cathode surface, the reduction of Co is promoted by the surface enrichment of its corresponding adsorbed metal hydroxide ions. Meanwhile, the higher P content of the Co–Ni–P-II film than that of the Co–Ni–P-I film is also observed. This finding might be caused by the phenomenon that Sc- CO_2 emulsion electrodeposition increases the H^+ concentration in the plating solution [26]. The reaction mechanism of Co–Ni–P electrodeposits is described below. Electrodeposition of individual Co and Ni metals can be simply depicted by the following equation:



Non-metal P cannot be deposited alone without Co and Ni. It can be readily deposited with iron group metals, a phenomenon known as induced co-deposition. According to the earlier studies, the incorporation of phosphorous, in principle, can be described by the following equation [27]:



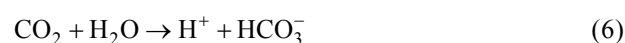
From reactions (1), (2) and (3), we can get the following equation:



Simultaneous hydrogen evolution occurs:



The H^+ concentration is increased in the Sc- CO_2 emulsion electrolyte by the reaction:



According to reaction (7), reaction (3) is promoted:



Hence, higher amount of P is co-deposited in the Co–Ni–P films by reaction (4).

XRD patterns show that the Co–Ni–P films display typical pattern of crystalline structure in spite of the electrodeposition techniques, because of the low P content of the as-plated films [28]. The Co–Ni–P-I film displays a strong hcp (110) diffraction peak and a relatively low intensity of hcp (002) diffraction peak. In contrast, the Co–Ni–P-II film exhibits a strong hcp (100) diffraction peak. The preferred orientation of the crystal growth on electrodeposition is affected by electroplating conditions including electrolyte composition, temperature, pH, current density, stirring and organic additions [29,30]. In this investigation, the preferred orientation of hcp (110) for the Co–Ni–P-I film prepared in conventional aqueous bath is changed to be hcp (100) for the Co–Ni–P-II film deposited in Sc–CO₂ emulsified bath, which might be attributed to the introduction of Sc–CO₂ fluid at high pressure. LUO et al [21] and YOO et al [31] found that a phase transition occurred for the Co film at higher pressure and ambient temperature. The average grain size calculations using the Scherrer's formula show that the Co–Ni–P films are both in nanocrystalline structure. A slight increase in the grain size is observed for the Co–Ni–P-II films as a consequence of higher P content [32].

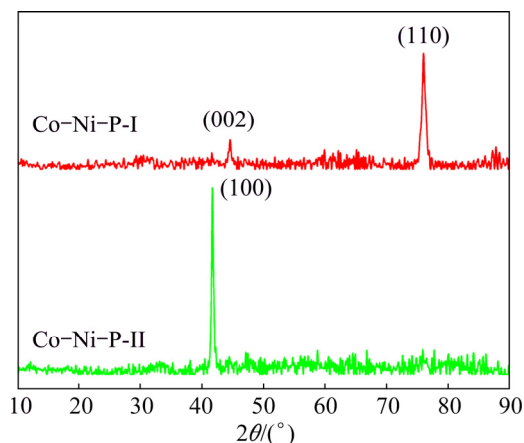


Fig. 3 XRD patterns of Co–Ni–P films electrodeplated by different techniques

Previous study reported a special characteristic named periodic plating when Sc–CO₂ emulsion was applied in electrodeplating reaction [19]. An illustration of periodic plating is shown in Fig. 4. During the electrodeposition process in emulsified Sc–CO₂ bath, the aqueous electrolyte, Sc–CO₂ fluid and non-ionic surfactant are in a dynamic emulsified form in the reaction chamber with the presence of agitation. ROCHA

et al [33] reported that the dynamic emulsion of a saline solution with Sc–CO₂ contains numerous micelles with radii in the range of several micrometers. Micelles can depart within the dynamic system, as shown in Fig. 4. When the aqueous electrolyte comes in contacts with the cathode, the nucleation and the crystal growth occur, and crystal growth stops when Sc–CO₂ fluid comes in contacts with the cathode, because electrical conductivity and solubility of metal salts are low in Sc–CO₂. In the meantime, H₂ desorption occurs when the Sc–CO₂ fluid comes in contacts with the cathode, due to the high solubility of H₂ in Sc–CO₂. Moreover, the lower viscosity of Sc–CO₂ emulsion leads to the higher mobility of the reactants in the reaction medium and results in higher nucleus density. The enhanced nucleus density and H₂ desorption result in the smooth surface and compact structure of the Co–Ni–P film deposited in emulsified Sc–CO₂ bath (Fig. 1).

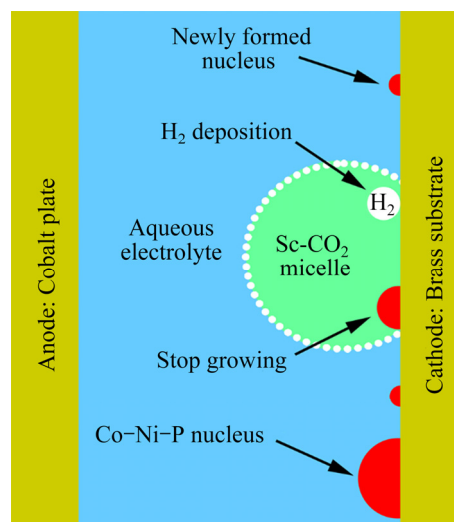


Fig. 4 Illustration of periodic plating of electrodeposition in emulsified Sc–CO₂ bath

3.2 Wear and corrosion behaviors of Co–Ni–P films

Figure 5(a) shows the typical friction coefficient curves of the Co–Ni–P films produced by different electrodeposition techniques. The friction coefficients of the Co–Ni–P films increase to a certain value and maintain at this level until the end of the test. The Co–Ni–P-II film displays more stable friction coefficient than the Co–Ni–P-I film with increasing sliding distance. Besides, it can be seen that the Co–Ni–P-II film shows higher average friction coefficient than the Co–Ni–P-I film. The microhardness and wear rate of the Co–Ni–P films are shown in Fig. 5(b). The Co–Ni–P-II film exhibits higher microhardness of 5.4 GPa than 4.1 GPa for the Co–Ni–P-I film, which might be attributed to the incorporation of higher P content in the Co–Ni–P-II film [32]. Figure 5(b) also shows that the wear rate of the

as-prepared Co–Ni–P-II film is $5.75 \times 10^{-6} \text{ mm}^3/(\text{N} \cdot \text{m})$, which is much lower than $15.27 \times 10^{-6} \text{ mm}^3/(\text{N} \cdot \text{m})$ for the Co–Ni–P-I film. This reveals that the Co–Ni–P film produced in emulsified Sc-CO_2 bath possesses better wear resistance than the one prepared in conventional aqueous bath at atmosphere. The lower wear rate of the Co–Ni–P-II film might be attributed to its higher microhardness (Fig. 5(b)). According to the classical Archard's law, the wear rate is proportional to the inverse microhardness of materials under the same wear conditions [34].

SEM images of the worn surfaces for the Co–Ni–P films sliding against GCr15 steel ball are shown in Fig. 6. The SEM images of the worn surfaces are consistent with the results shown in Fig. 5(b). The wear scar of the Co–Ni–P-I film (Figs. 6(a) and (b)) is wider than that of the Co–Ni–P-II film (Figs. 6(c) and (d)). Additionally, severe fatigue wear seems to be the major wear mechanism for the Co–Ni–P-I film, because most of micro-cracks are observed on its worn surface. The micro-cracks are initiated from micro-defects, such as voids/pinholes on the surface or subsurface (Fig. 1) after

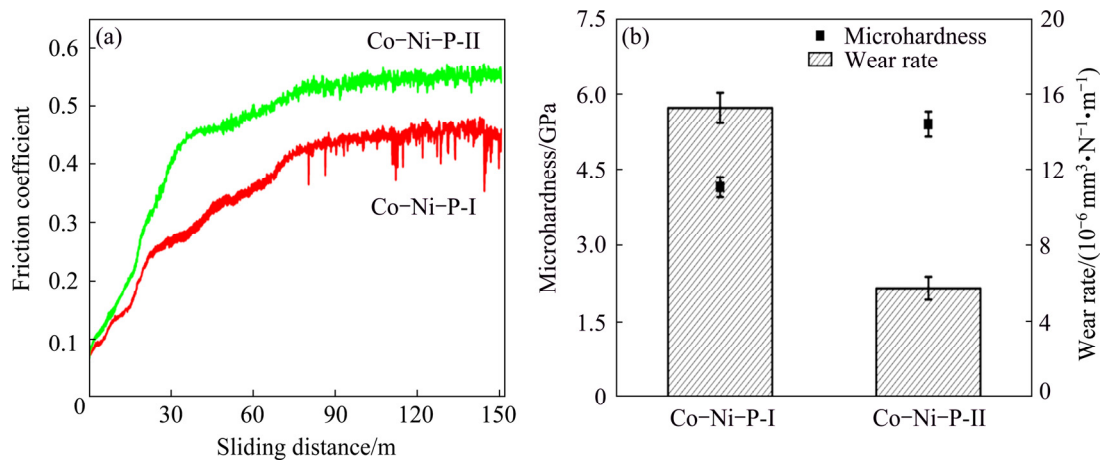


Fig. 5 Typical friction coefficient curves (a), microhardness and wear rate (b) of Co–Ni–P films electroplated by different techniques

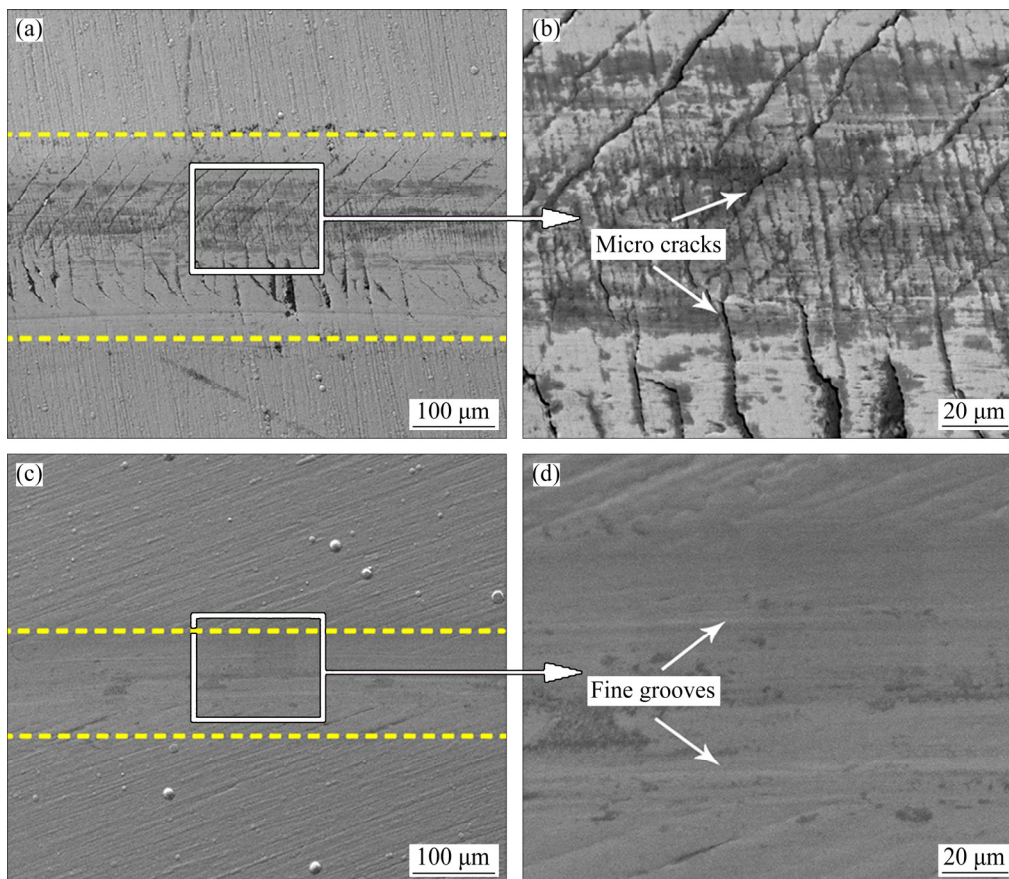


Fig. 6 SEM images of worn surfaces of Co–Ni–P films electroplated by different techniques: (a, b) Co–Ni–P-I; (c, d) Co–Ni–P-II

a certain number of repeated cycles, due to the high contact pressure. As the wear test continues, the fatigue cracks propagate in the worn zone, especially around the edge of wear scar (Fig. 6(b)), due to the high strain, large deformation and local stress concentration. For the Co–Ni–P–II film, the worn surface is relatively smooth and featured with fine grooves along the sliding direction without signs of severe plastic deformation and adhesion (Figs. 6(c) and (d)), which might be due to its even surface, compact structure and high microhardness (Figs. 1 and 5(b)). These characteristics of the worn surfaces indicate the change from severe fatigue wear for the Co–Ni–P–I film to slight abrasive wear for the Co–Ni–P–II film.

SEM images of the worn surface on the counterpart balls sliding against the Co–Ni–P films are shown in Fig. 7. Circular wear scars and accumulations of wear debris are clearly visible on the counterpart steel balls. EDS analysis demonstrates that the accumulated wear debris on the counterpart steel balls is mainly composed of Co, Ni and P elements from the transferred Co–Ni–P films during the sliding process. It is worth noting that the counterpart ball sliding against Co–Ni–P–I film

displays larger wear scar diameter and more accumulated wear debris on its surface than that sliding against Co–Ni–P–II film (Figs. 7(a) and (c)). Additionally, severe adhesion wear is observed on the counterpart ball sliding against the Co–Ni–P–I film (Fig. 7(b)). Obvious signs of deformation and delamination are observed on the worn surface of this counterpart ball, caused by the rough surface and low microhardness of the Co–Ni–P–I film. The high friction stress can give rise to the delamination of this film and makes it easier transfer to the counterpart steel ball.

The potentiodynamic polarization curves of the Co–Ni–P films measured in 3.5% NaCl solution are described in Fig. 8(a). The corrosion potential (φ_{corr}), corrosion current density (J_{corr}) and corrosion rate calculated using the program CorShow from the potentiodynamic polarization curves are listed in Table 3. Compared with the Co–Ni–P–I film (–503.8 mV), the φ_{corr} of the Co–Ni–P–II film shifts in the positive direction to –363.8 mV, which is about 140 mV more positive than that of the Co–Ni–P–I film. The Co–Ni–P–II film exhibits lower J_{corr} and corrosion rate, whose value are about half those of the Co–Ni–P–I film.

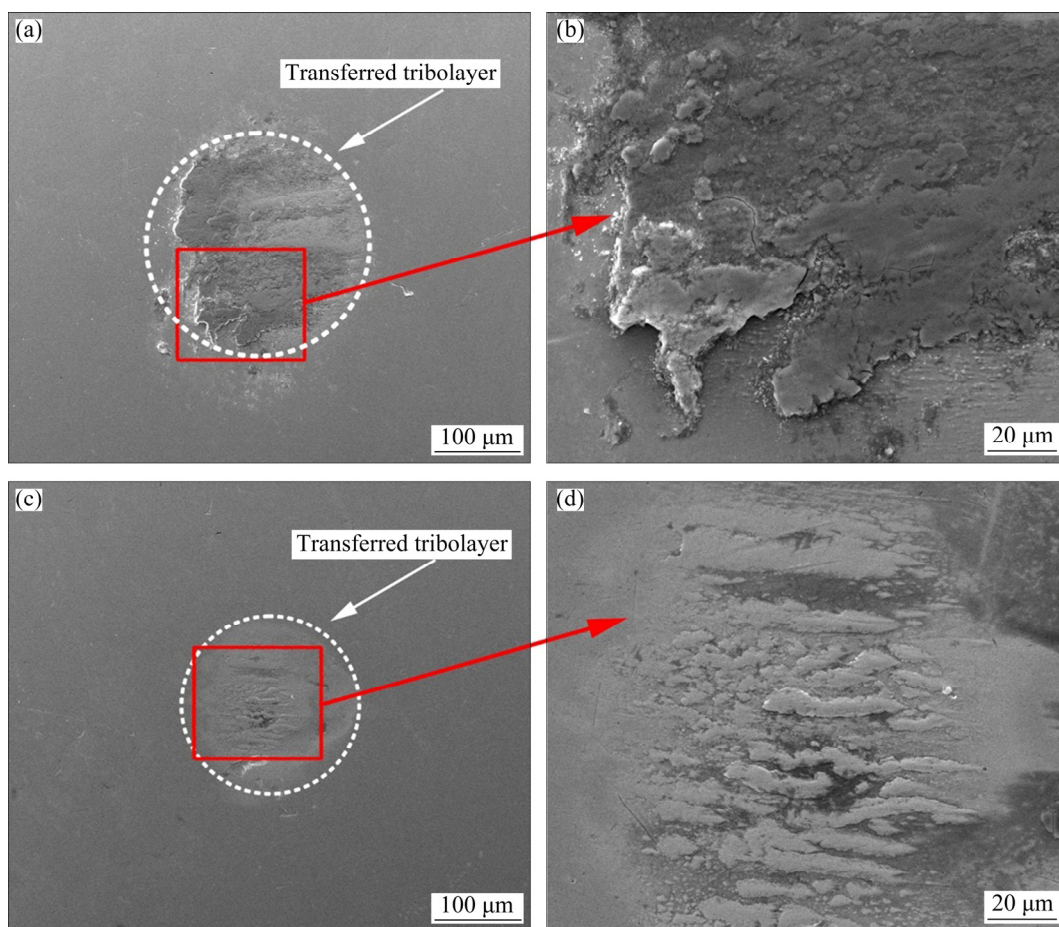


Fig. 7 SEM images of worn surfaces of counterpart balls sliding against Co–Ni–P films electroplated by different techniques: (a, b) Co–Ni–P–I; (c, d) Co–Ni–P–II

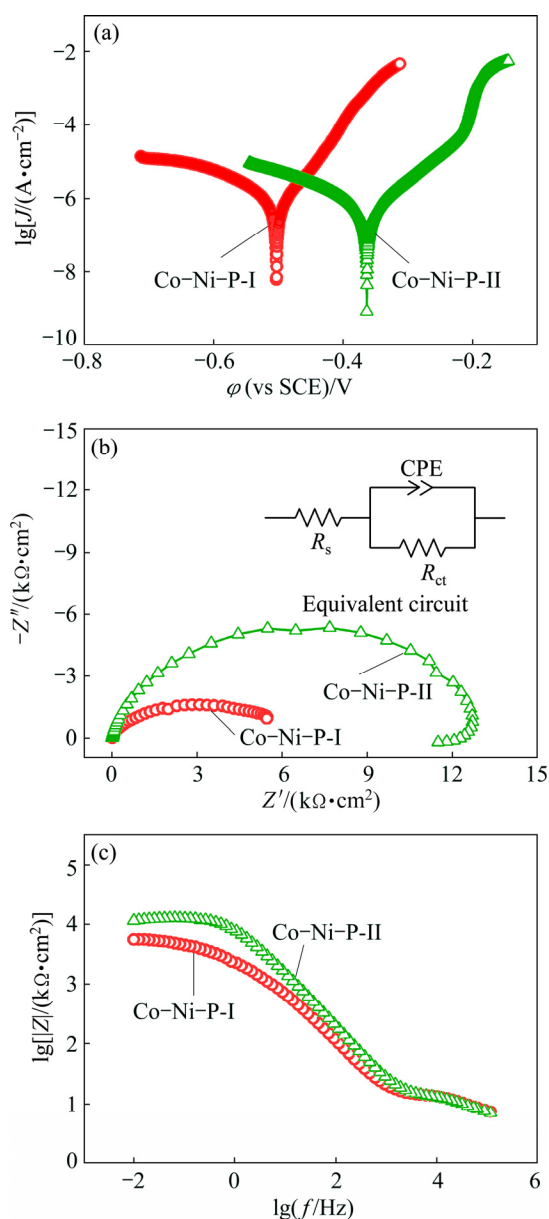


Fig. 8 Potentiodynamic polarization curves (a), Nyquist plots (b) and Bode plots (c) of Co–Ni–P films measured in 3.5% NaCl solution (Insert in (b): Equivalent circuit employed to fit impedance data)

Table 3 Corrosion potential (ϕ_{corr}), corrosion current density (J_{corr}) and corrosion rate of Co–Ni–P films measured in 3.5% NaCl solution

Sample	$\phi_{\text{corr}}/\text{mV}$	$J_{\text{corr}}/(\text{A}\cdot\text{cm}^{-2})$	Corrosion rate/ $(\text{mm}\cdot\text{a}^{-1})$
Co–Ni–P–I	–503.8	9.71×10^{-7}	4.99×10^{-3}
Co–Ni–P–II	–363.8	5.19×10^{-7}	2.67×10^{-3}

The results show that the Co–Ni–P film prepared in emulsified Sc–CO₂ bath presents better corrosion resistance than the one fabricated by conventional electrodeposition technique due to its more positive ϕ_{corr} , lower J_{corr} and lower corrosion rate.

As a powerful, complementary electrochemical technique, electrochemical impedance spectroscopy is also used to evaluate the corrosion properties of the deposited films. Figures 8(b) and (c) show the Nyquist plots and Bode plots of the Co–Ni–P films measured in 3.5% NaCl solution, respectively. The equivalent circuit inserted in Fig. 8(b) is proposed to fit the experimental impedance data using Z_{view} software. In this circuit, R_s is electrolyte resistance between the reference electrode and the working electrode, R_{ct} means the charge transfer resistance and CPE is the constant phase element of the electrical double layer. The diameter of the capacitive loop in the Nyquist plots represents the polarization resistance of the working electrode. As shown in Fig. 8(b), the diameter of the Nyquist loop in the Co–Ni–P–II film is significantly larger than that of the Co–Ni–P–I film. The impedance value of the Co–Ni–P–II film is around $12.6\times 10^3 \Omega\cdot\text{cm}^2$ that is more than twice the value of the Co–Ni–P–I film ($5.1\times 10^3 \Omega\cdot\text{cm}^2$). In addition, Fig. 8(c) depicts that the Co–Ni–P–II film possesses a higher impedance modulus than the Co–Ni–P–I film at low frequency. In other words, both Nyquist plot and Bode diagram results confirm that the Co–Ni–P film produced in Sc–CO₂ emulsion bath exhibits better corrosion resistance in 3.5% NaCl solution than the one produced in conventional aqueous bath at atmosphere.

The remarkable corrosion behavior of the Co–Ni–P–II film might be attributed to its smooth surface and compact structure (Fig. 1). A smoother surface means smaller area exposed to the attack of anodic dissolution, and the compact structure can prevent the corrosive medium from eroding the film or reaching the interface of film and substrate. Besides, the P content has a significant effect on the corrosion resistance of the film. High P-content films are more homogeneous and lack definite grain boundaries, possible locations of preferential dissolution and this may account in part for the higher corrosion resistance [35]. As a result, it can be concluded that smoother surface, more compact structure and higher P content correspond to the improved corrosion resistance for the Co–Ni–P film fabricated by electroplating with Sc–CO₂ emulsion.

4 Conclusions

1) The Co–Ni–P film prepared in emulsified Sc–CO₂ bath displays a more compact structure and higher P content. The hcp (110) preferred orientation for the Co–Ni–P film deposited in conventional aqueous bath is changed to be hcp (100) for the one produced in emulsified Sc–CO₂ bath.

2) The periodic plating of the electrodeposition in Sc–CO₂ emulsion at high pressure enhances the hydrogen

desorption and nucleus density, resulting in the smoother surface, more compact structure and the change of crystal phase structures for the as-plated Co–Ni–P film.

3) The Co–Ni–P film electrodeposited with Sc–CO₂ emulsion exhibits much better anti-wear properties and corrosion resistance than the film electrodeposited by conventional method, which might be attributed to smoother surface, more compact structure and higher microhardness of the film produced with the aid of Sc–CO₂.

References

- [1] LU Ke, LU Jian. Nanostructured surface layer on metallic materials induced by surface mechanical attrition treatment [J]. *Materials Science and Engineering A*, 2004, 375: 38–45.
- [2] SRIVASTAVA M, ANANDAN C, GRIPS V K W. Ni–Mo–Co ternary alloy as a replacement for hard chrome [J]. *Applied Surface Science*, 2013, 285: 167–174.
- [3] MENG Zhen-qiang, LI Xi-bin, XIONG Yong-jun, ZHAN Jing. Preparation and tribological performances of Ni–P-multi-walled carbon nanotubes composite coatings [J]. *Transactions of Nonferrous Metals Society of China*, 2012, 22: 2719–2725.
- [4] ZHOU Ya-ru, ZHANG Shan, NIE Lin-lin, ZHU Ze-jie, ZHANG Jian-qing, CAO Fa-he, ZHANG Jun-xi. Electrodeposition and corrosion resistance of Ni–P–TiN composite coating on AZ91D magnesium alloy [J]. *Transactions of Nonferrous Metals Society of China*, 2016, 26: 2976–2987.
- [5] WANG Li-ping, GAO Yan, XUE Qun-ji, LIU Hui-wen, XU Tao. A novel electrodeposited Ni–P gradient deposit for replacement of conventional hard chromium [J]. *Surface and Coatings Technology*, 2006, 200: 3719–3726.
- [6] ZHOU Hai-hui, LIAO Zuo-wei, FANG Chen-xu, LI Huan-xin, FENG Bin, XU Song, CAO Guo-fei, KUANG Ya-fei. Pulse electroplating of Ni–W–P coating and its anti-corrosion performance [J]. *Transactions of Nonferrous Metals Society of China*, 2018, 28: 88–95.
- [7] FANG Meng, HU Ling, YANG Lei, SHI Chang-dong, WU Yu-cheng, TANG Wen-ming. Electroless plating and growth kinetics of Ni–P alloy film on SiC_p/Al composite with high SiC volume fraction [J]. *Transactions of Nonferrous Metals Society of China*, 2016, 26: 799–805.
- [8] MA C, WANG S C, WANG L P, WALSH F C, WOOD R J K. The role of a tribofilm and wear debris in the tribological behaviour of nanocrystalline Ni–Co electrodeposits [J]. *Wear*, 2013, 306: 296–303.
- [9] LIU W L, HSIEH S H, CHEN W J, HSU Y C. Growth behavior of electroless Ni–Co–P deposits on Fe [J]. *Applied Surface Science*, 2009, 255: 3880–3883.
- [10] MA C, WANG S C, WANG L P, WALSH F C, WOOD R J K. The electrodeposition and characterisation of low-friction and wear-resistant Co–Ni–P coatings [J]. *Surface and Coatings Technology*, 2013, 235: 495–505.
- [11] LU Xun-yu, ZHAO Chuan. Electrodeposition of hierarchically structured three-dimensional nickel–iron electrodes for efficient oxygen evolution at high current densities [J]. *Nature Communications*, 2015, 6: 1–7.
- [12] ZHOU Mei-peng, MAI Yong-jin, LING Hong-jie, CHEN Fu-xian, LIAN Wei-qi, JIE Xiao-hua. Electrodeposition of CNTs/copper composite coatings with enhanced tribological performance from a low concentration CNTs colloidal solution [J]. *Materials Research Bulletin*, 2018, 97: 537–543.
- [13] BOSTANI B, AHMADI N P, YAZDANI S, ARGHAVANIAN R. Co-electrodeposition and properties evaluation of functionally gradient nickel coated ZrO₂ composite coating [J]. *Transactions of Nonferrous Metals Society of China*, 2018, 28: 66–76.
- [14] NICHOLSON E L, KHAN M R. Microstructure and magnetic properties of electroless plated Co–Ni–P and Co–P thin films for magnetic recording [J]. *Journal of the Electrochemical Society*, 1986, 133: 2342–2345.
- [15] LI Yong-jie, WANG Rui, QI Feng-ming, WANG Chun-ming. Preparation, characterization and microwave absorption properties of electroless Ni–Co–P-coated SiC powder [J]. *Applied Surface Science*, 2008, 254: 4708–4715.
- [16] PODESTÁ J J, PIATTI R C V, ARVIA A J. The influence of iridium, ruthenium and palladium on the electrochemical behaviour of Co–P and Ni–Co–P base amorphous alloys for water electrolysis in KOH aqueous solutions [J]. *International Journal of Hydrogen Energy*, 1995, 20: 111–122.
- [17] KE Jie, SU Wen-ta, HOWDLE S M, GEORGE M W, COOK D, MAGDA P A, BARTLETT P N, ZHANG Wen-jian, CHENG Fei, LEVASON W. Electrodeposition of metals from supercritical fluids [J]. *Proceedings of the National Academy of Sciences*, 2009, 106: 14768–14772.
- [18] HOWDLE S M, BAGRATASHVILI V N. The effects of fluid density on the rotational Raman spectrum of hydrogen dissolved in supercritical carbon dioxide [J]. *Chemical Physics Letters*, 1993, 214: 215–219.
- [19] CHANG T F M, SONE M, SHIBATA A, ISHIYAMA C, HIGO Y. Bright nickel film deposited by supercritical carbon dioxide emulsion using additive-free Watts bath [J]. *Electrochimica Acta*, 2010, 55: 6469–6475.
- [20] CHIU Shih-yi, CHUNG Sung-ting, LIN Cheng-yang, TSAI Wen-ta. Electrodeposition of Ni–Al₂O₃ composite coatings employing supercritical CO₂ baths [J]. *Surface and Coatings Technology*, 2014, 247: 68–73.
- [21] LUO Xun, CHEN Chun-yi, CHANG T F M, HOSODA H, SONE M. Crystal growth of cobalt film fabricated by electrodeposition with dense carbon dioxide [J]. *Journal of the Electrochemical Society*, 2015, 162: D423–D426.
- [22] LIU Can-sen, SU Feng-hua, LIANG Ji-zhao. Nanocrystalline Co–Ni alloy coating produced with supercritical carbon dioxide assisted electrodeposition with excellent wear and corrosion resistance [J]. *Surface and Coatings Technology*, 2016, 292: 37–43.
- [23] YOSHIDA H, SONE M, WAKABAYASHI H, YAN Hao, ABE K, TAO Xu-tang, MIZUSHIMA A, ICHIHARA S, MIYATA S. New electroplating method of nickel in emulsion of supercritical carbon dioxide and electroplating solution to enhance uniformity and hardness of plated film [J]. *Thin Solid Films*, 2004, 446: 194–199.
- [24] CHUNG Sung-ting, TSAI Wen-ta. Nanocrystalline Ni–C electrodeposits prepared in electrolytes containing supercritical carbon dioxide [J]. *Journal of the Electrochemical Society*, 2009, 156: D457–D461.
- [25] BAI A, HU Chi-chang. Composition controlling of Co–Ni and Fe–Co alloys using pulse-reverse electroplating through means of experimental strategies [J]. *Electrochimica Acta*, 2005, 50: 1335–1345.
- [26] UCHIYAMA H, SONE M, SHIBATA A, HIGO Y. Effects of CO₂ on Ni–P electroless plating in an emulsion of supercritical CO₂ [J]. *Journal of the Electrochemical Society*, 2010, 157: D550–D552.
- [27] DJOKIĆ S S. Electrodeposition of amorphous alloys based on the iron group of metals [J]. *Journal of the Electrochemical Society*, 1999, 146: 1824–1828.
- [28] MA C, WANG S, WALSH F C. The electrodeposition of nanocrystalline cobalt-nickel-phosphorus alloy coatings: A review [J]. *Transactions of the IMF*, 2015, 93: 275–280.

- [29] CZERWINSKI F, SZPUNAR J A. Controlling the surface texture of nickel for high temperature oxidation inhibition [J]. Corrosion Science, 1999, 41: 729–740.
- [30] WU Wang-ping, ELIAZ N, GILEADI E. The effects of pH and temperature on electrodeposition of Re–Ir–Ni coatings from aqueous solutions [J]. Journal of the Electrochemical Society, 2015, 162: D20–D26.
- [31] YOO C S, CYNN H, DERLIND P S, IOTA V. New β (fcc)-cobalt to 210 GPa [J]. Physical Review Letters, 2000, 84: 4132–4135.
- [32] COJOCARU P, MAGAGNIN L, GÓMEZ E, VALLÉS E. Electrodeposition of CoNi and CoNiP alloys in sulphamate electrolytes [J]. Journal of Alloys and Compounds, 2010, 503: 454–459.
- [33] ROCHA S R D P, PSATHAS P A, KLEIN E, JOHNSTON K P. Concentrated CO₂-in-water emulsions with nonionic polymeric surfactants [J]. Journal of Colloid and Interface Science, 2001, 239: 241–253.
- [34] WANG Li-ping, GAO Yan, XUE Qun-ji, LIU Hui-wen, XU Tao. Microstructure and tribological properties of electrodeposited Ni–Co alloy deposits [J]. Applied Surface Science, 2005, 242: 326–332.
- [35] VIADL-SICART S, BROUWER O R, TAN I B, VALDÉD-OLMOS R A, MATHERON H M. Nickel phosphide: The effect of phosphorus content on hydrogen evolution activity and corrosion resistance in acidic medium [J]. Journal of Materials Chemistry A, 2014, 2: 17435–17445.

超临界二氧化碳乳液电沉积制备耐磨防腐 Co–Ni–P 镀层

刘灿森^{1,2}, 苏峰华¹, 梁基照¹

1. 华南理工大学 机械与汽车工程学院, 广州 510640;

2. 广东工业大学 材料与能源学院, 广州 510006

摘要: 为避免析氢反应带来的缺陷以及提高传统水浴电沉积镀层的抗磨耐蚀性能, 采用超临界二氧化碳(Sc-CO₂)乳液电沉积制备三元 Co–Ni–P 合金镀层, 并与传统方法制备的镀层的显微组织、耐蚀性和摩擦学性能进行对比研究。结果表明, Sc-CO₂ 乳液电沉积制备的 Co–Ni–P 镀层结构更加致密, 镀层的择优取向由传统水镀液制备的 hcp (110)变为 Sc-CO₂ 乳液制备的 hcp (100); 此外, Sc-CO₂ 乳液电沉积能显著提高 Co–Ni–P 镀层的显微硬度、耐蚀性和摩擦学性能。

关键词: Co–Ni–P 镀层; 电沉积; 超临界二氧化碳; 磨损; 腐蚀

(Edited by Bing YANG)